

COVER PAGE

Document downloaded by @DAEL

Fri Nov 6 14:24:32 2026
For personal use

When automatic English translation is provided, only the original document is authentic.
The EAA cannot be held responsible of any translation error

Bibliographical reference

Development of 3D Acoustic Multi-Domains Analysis Using an Indirect Energy Flow Boundary Element Method, Jong-Do Kim, Sung-Mok Hwang, . Hyuk-Kwun and Bong-Jae Kim, Acta Acustica **vol. 103** (Number 3), 2017, pp. 523-530

DOI
https://doi.org/10.3813/AAA.919080

Acta Acustica united with Acustica
Vol. 103 (2017) 523 – 530

Technical and Applied Papers
DOI 10.3813/AAA.919080

Development of 3D Acoustic Multi-Domains Analysis Using an Indirect Energy Flow Boundary Element Method

Jong-Do Kim, Sung-Mok Hwang, Hyuk-Kwun, Bong-Jae Kim
Central Research Institute, Samsung Heavy Industries Co. Ltd, Seongnam-si, Republic of Korea.
jd7.kim@samsung.com

Summary
Energy flow analysis has been developed and studied by many researchers to analyze acoustic energy in the medium to high frequency ranges. In this paper, a method to solve the 3D acoustic multi-domain problem by adopting an indirect approach to the EFBEM (Energy Flow Boundary Element Method) is proposed. A joint matrix comprised of power transmission and reflection coefficients is used to describe the energy exchanges between domains and absorption coefficients are applied to consider an energy absorbing boundary condition. Finally, coupled small reverberation rooms and a mock-up system of ship cabins were analyzed using the method to compare the numerical analysis with the experimental results. They show good agreement, thereby validating the method. The indirect EFBEM method allows us to use spherical wave Green's functions, which are not available in the direct method. Therefore, it is expected that the method can be applied to almost any acoustic multi-domain situation, from room to room cases to radiation problems.

PACS no. 43.20.-f, 43.55.-n

1. Introduction

Predicting noise and vibration levels is very important to engineers in, for instance, the automotive, shipbuilding and aircraft industries because noise and vibration problems are negatively related to passengers' comfort. Many researchers have tried to develop better analysis methods with more efficient calculations by taking advantage of technology like parallel computing, making numerical analysis more popular and more accurate than before.

Numerical methods for noise and vibration analysis have usually been classified by frequency range. The well-known conventional methods like the FEM (finite element method) and the BEM (boundary element method) are appropriate for low frequency problems because they are based on the wave propagation theory. However, as the frequency increases, the wavelength decreases, therefore the mesh size needs to be smaller to accurately describe wave motion. Generally, 6–8 elements can be modeled within a wavelength to obtain reliable results, but it becomes difficult to use conventional methods in medium to high frequency ranges.

SEA (statistical energy analysis) was developed by Lyon [1] to predict noise and vibration at high frequencies when the modal density is high enough. It provides a space and time-averaged energy density in a subsystem. Basically, energy-based methods have no constraints on element size because the phase of the waves are not considered, and so SEA has been widely used to predict high frequency acoustic energy. However, it has some limitations: first, it cannot provide the spatial energy distribution of the subsystems, and second, it is valid only when the modal density is high enough.

Ray tracing can also be a good alternative for room acoustics problems in high frequency ranges. It is a very straightforward method to calculate interior noise and it is effective to analyze the impulse response in a room. However, it takes lots of computational efforts to obtain a steady state room interior noise field when a large number of rays and reflections are considered.

To overcome the weaknesses of the above methods, EFA (energy flow analysis) was introduced by Belov *et al.* [2]. It is also an energy-based method similar to SEA but it considers spatial energy distribution and energy flow (intensity). Moreover, the conventional FEM and BEM formulations can easily be applied to EFA because its energy governing equation is analogous to the steady state heat conduction equation. In the late 1980's, Nefske and Sung [3] applied FEM to the vibrational energy governing equation from the Euler-Bernoulli beam theory, and Wohlever and Bernhard [4] additionally studied vibrational power flow in rods and the Euler-Bernoulli beam. Bouthier and Bernhard [5, 6] expanded on the work of Wohlever and Bernhard by applying the energy model to membranes, the Kirchhoff plate, and acoustic cavities.

Received 21 August 2016,
accepted 19 March 2017.

© S. Hirzel Verlag · EAA

Document downloaded by @DAEL, 2026-11-06 14:24:34 - personal use only

Smith [7] suggested a hybrid method to predict vibrational response of a point loaded plate. It computes the direct field and the reverberant field separately, and LeBot [8] developed a vibro-acoustic model for the analysis of multi-dimensional systems like plates and acoustic cavities. Furthermore, Park *et al.* [9] studied energy flow models for in-plane waves in isotropic thin plates and for flexural waves in orthotropic thin plates, and an energy flow model for a reinforced plate was suggested by Seo and Hong [10].

On the other hand, Lee *et al.* [11] applied the BEM to the EFA energy governing equation, and Kwon *et al.* [12, 13] derived the spherical wave energy governing equation using the far field assumption by implementing an indirect BEM for the governing equation. Wang *et al.* [14] also suggested energy boundary element analysis (EBEA) formulations for the sound radiation problem at high frequencies under the incoherent intensity boundary condition. Efforts to predict directivity of sound propagation in an energy-based method were carried out by Rouser and Franzoni [15], and Besset *et al.* [16], while Chappell *et al.* [17] introduced dynamic energy analysis (DEA) based on the Chebyshev expansion to analyze coupled acoustic systems at high frequencies and showed its robustness by comparison with FEM and SEA.

For multi-domains problems, a direct EFBEM was considered by Hong *et al.* [18, 19, 20, 21, 22], and in this case, the integral equation is derived using the divergence theorem, thus is available only for closed domains. Moreover, its governing equation is derived with the plane wave assumption, which has limitations for general acoustic problems, e.g. sound radiation.

In this study, a new approach using an indirect EFBEM to analyze 3D multi-domain problems is suggested. Energy flow between adjacent domains is expressed in a joint matrix comprised of power transmission and reflection coefficients in common partitions. The energy absorption by the enclosed surfaces of each domain is considered by applying absorption coefficients on the boundary. Moreover adopting Green's functions for spherical waves as well as plane waves makes this method useful for various acoustic coupling cases.

2. Methodology

2.1. The energy governing equation

The acoustic energy governing equation for a spherical wave is derived using the far field ($kr \gg 1$) and low damping assumptions [12, 13],

$$-\frac{c_g^2}{\eta\omega}\nabla\cdot\left\{\frac{1}{r^2}\frac{\mathrm{d}}{\mathrm{d}r}\left(r^2\langle e\rangle\right)\boldsymbol{r}\right\}+\eta\omega\langle e\rangle=\langle\pi_{\mathrm{in}}\rangle. \tag{1}$$

where $\langle..\rangle$ means a time-averaged value, r is the distance from the source to the receiver, $\boldsymbol{r}$is a direction vector, η is the damping loss factor, and $\langle\pi_{\mathrm{in}}\rangle$ is the external input power to the subsystem. As the solution for Equation (1), Green's function G is substituted for $\langle e\rangle$ in Equation (2),

$$\nabla\cdot\left\{\frac{1}{r^2}\frac{\mathrm{d}}{\mathrm{d}r}\left(r^2G\right)\boldsymbol{r}\right\}-\eta^2k^2G=\delta(r), \tag{2}$$

where $\delta(r)$ is the Dirac delta function and k is the acoustic wave number. G is expressed in Equation (3) as [12, 13]

$$G(r)=\frac{1}{4\pi c_g r^2}\mathrm{e}^{-\eta kr}, \tag{3}$$

where c_g is the group velocity. Using Equation (3) the time-averaged acoustic energy density at distance r can be obtained. For intensity, Green's function F is given as [12, 13]

$$F(r)=\frac{1}{4\pi r^2}\mathrm{e}^{-\eta kr}. \tag{4}$$

2.2. Indirect EFBEM

The indirect approach to the EFBEM is used in this research as previously mentioned. The basic concept of the indirect method is that a real system is embedded in an infinite acoustic field, and the reverberation field can be expressed by a number of fictitious sources distributed on the boundary surface of the real system [23]. The acoustic energy density at a specific point can be obtained by adding the energy densities from the real acoustic source and the fictitious sources because the sound waves have linearity. As a result, the energy density and the acoustic intensity can be respectively expressed as

$$\begin{aligned}e(\boldsymbol{x}) &= \int_S G(|\boldsymbol{x}-\boldsymbol{\xi}|)\,\Phi(\boldsymbol{\xi})\,\mathrm{d}S(\boldsymbol{\xi})\\ &\quad+\int_V G(|\boldsymbol{x}-\boldsymbol{z}|)\,\Pi_{\mathrm{in}}(\boldsymbol{z})\,\mathrm{d}V(\boldsymbol{z}),\end{aligned} \tag{5}$$

$$\begin{aligned}q(\boldsymbol{x}) &= \int_S F(|\boldsymbol{x}-\boldsymbol{\xi}|)\,\Phi(\boldsymbol{\xi})\,\mathrm{d}S(\boldsymbol{\xi})\\ &\quad+\int_V F(|\boldsymbol{x}-\boldsymbol{z}|)\,\Pi_{\mathrm{in}}(\boldsymbol{z})\,\mathrm{d}V(\boldsymbol{z}),\end{aligned} \tag{6}$$

where G and F are Green's functions for energy density and intensity, respectively; V is the 3D domain; S denotes the surface boundary; $\boldsymbol{x}$, $\boldsymbol{\xi}$ and $\boldsymbol{z}$ are the position vectors of the receivers in the domain, the fictitious sources on the boundary, and the physical acoustic sources, respectively, and $\Phi(\boldsymbol{\xi})$ is the strength of the fictitious sources. The first integrals on the right hand side of Equations (5) and (6) represent the energy density and intensity reproduced by boundary surfaces, i.e. the reverberation field, and the second integrals are the contributions of the physical acoustic sources.

The boundary surfaces need to be discretized to solve the boundary integral equations of Equations (5) and (6), then they can respectively be rewritten in matrix form as

$$\{e\}_{l\times1} = [G]_{l\times m}\{\Phi\}_{m\times1}+[G]_{l\times n}\{\Pi\}_{n\times1}, \tag{7}$$

$$\{q\}_{l\times1} = [F]_{l\times m}\{\Phi\}_{m\times1}+[F]_{l\times n}\{\Pi\}_{n\times1}, \tag{8}$$

where l is the number of receiving points, m is the number of boundary surface elements, and n is the number of acoustic sources. The matrices and are comprised of values of Green's function for the energy density and intensity, respectively.

Document downloaded by @DAEL, 2026-11-06 14:24:34 - personal use only

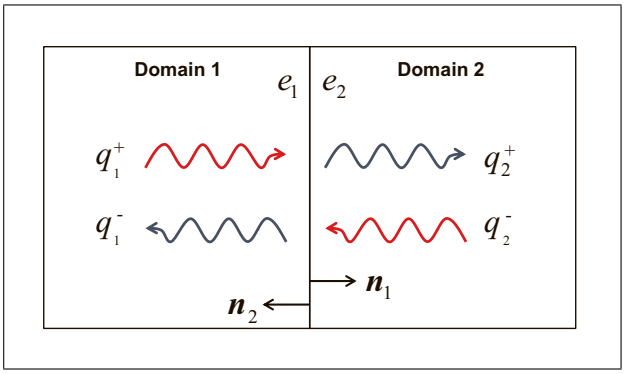


Figure 1. Interface condition of 3D acoustic multi-domains.

2.3. Multi-domain analysis

2.3.1. Coupling relationship

Energy flow between 3D acoustic domains is shown in Figure 1 where $\boldsymbol{n}$ indicates the normal vectors, and q^+ and q^- are the outward and inward intensities, respectively. The domains can be divided by the different impedances of liquid and solid materials. The following equations are used to derive the energy flow relationships between the two domains [18],

$$q_1 = q_1^+ - q_1^-, \tag{9}$$
$$q_2 = q_2^+ - q_2^-, \tag{10}$$
$$\{q\} = \{q^+\} - \{q^-\}, \tag{11}$$
$$e_1 = e_1^+ + e_1^-, \tag{12}$$
$$e_2 = e_2^+ + e_2^-, \tag{13}$$
$$\{e\} = \{e^+\} + \{e^-\}, \tag{14}$$

where e^+ and e^- are the outgoing and incoming components of the energy densities, respectively. The intensities at the interface can be expressed as the differences between the outgoing and incoming intensities given by Equations (9)–(11) because they are vector quantities while the energy densities at the interface are the summation of outgoing and incoming components.

Generally, acoustic intensity is expressed in terms of group velocity and energy density, as shown in

$$q_i^+ = c_{gi} e_i^+, \tag{15}$$
$$q_i^- = c_{gi} e_i^-, \tag{16}$$

where c_{gi} is the group velocity of domain i. The following are their respective matrix forms:

$$\{q^+\} = [C]\{e^+\}, \tag{17}$$
$$\{q^-\} = [C]\{e^-\}, \tag{18}$$

where $[C]$ is the group velocity matrix given as

$$[C] = \begin{bmatrix} c_{g1} & 0 \\ 0 & c_{g2} \end{bmatrix}. \tag{19}$$

Considering the power transmission and reflection coefficients, the incoming intensities of each domain can be expressed in terms of their outgoing intensities. That is to say, the incoming intensity of domain 1, q_1^-, is the summation of the reflected intensity of domain 1, $r_{11}q_1^+$, and the transmitted intensity from domain 2, $\tau_{21}q_2^+$, where r_{11} is the power reflection coefficient of domain 1 and τ_{21} is the power transmission coefficient from domain 2 to domain 1. This also can be applied to the incoming intensity of domain 2 and they can be expressed as

$$q_1^- = \gamma_{11}q_1^+ + \tau_{21}q_2^+, \tag{20}$$
$$q_2^- = \tau_{12}q_1^+ + \gamma_{22}q_2^+, \tag{21}$$
$$\{q^-\} = [P]\{q^+\}, \tag{22}$$

where $[P]$ is the power transmission-reflection coefficients matrix expressed as

$$[P] = \begin{bmatrix} \gamma_{11} & \tau_{21} \\ \tau_{12} & \gamma_{22} \end{bmatrix}. \tag{23}$$

The relationship between the intensities and the energy densities at the common boundary of coupled domains needs to be derived to define the joint matrix. Using Equation (11), the net energy flow variables q_1 and q_2 at the common boundary surface between domains 1 and 2, respectively, can be expressed in terms of the outward intensities because the inward intensities can be rewritten with outward intensities, power transmission, and reflection coefficients. Therefore, it can be obtained as

$$\begin{aligned} \begin{Bmatrix} q_1 \\ q_2 \end{Bmatrix} &= \begin{Bmatrix} q_1^+ \\ q_2^+ \end{Bmatrix} - \begin{Bmatrix} q_1^- \\ q_2^- \end{Bmatrix} \\ &= \begin{Bmatrix} q_1^+ \\ q_2^+ \end{Bmatrix} - [P] \begin{Bmatrix} q_1^+ \\ q_2^+ \end{Bmatrix} \\ &= [I - P] \begin{Bmatrix} q_1^+ \\ q_2^+ \end{Bmatrix}, \end{aligned} \tag{24}$$

where $[I]$ is an identity matrix.

Multiplying Equation (24) by results in

$$\begin{aligned} [C] \begin{Bmatrix} e_1 \\ e_2 \end{Bmatrix} &= [C] \begin{Bmatrix} e_1^+ \\ e_2^+ \end{Bmatrix} + [C] \begin{Bmatrix} e_1^- \\ e_2^- \end{Bmatrix} \\ &= \begin{Bmatrix} q_1^+ \\ q_2^+ \end{Bmatrix} + \begin{Bmatrix} q_1^- \\ q_2^- \end{Bmatrix} \\ &= [I + P] \begin{Bmatrix} q_1^+ \\ q_2^+ \end{Bmatrix}. \end{aligned} \tag{25}$$

The outward intensities can be expressed in terms of the energy density and power transmission-reflection coefficients matrix $[P]$ as

$$\begin{Bmatrix} q_1^+ \\ q_2^+ \end{Bmatrix} = [I + P]^{-1} [C] \begin{Bmatrix} e_1 \\ e_2 \end{Bmatrix}. \tag{26}$$

Finally, the intensities at the common boundary surface can be defined in terms of the energy densities and the joint matrix $[J]$ as

$$\begin{aligned} \begin{Bmatrix} q_1 \\ q_2 \end{Bmatrix} &= [I - P][I + P]^{-1} [C] \begin{Bmatrix} e_1 \\ e_2 \end{Bmatrix} \\ &= [J] \begin{Bmatrix} e_1 \\ e_2 \end{Bmatrix}, \end{aligned} \tag{27}$$

Document downloaded by @DAEL, 2026-11-06 14:24:34 - personal use only

where $[J]$ is the joint matrix comprised of the power transmission-reflection coefficient matrix, the identity matrix, and the group velocity matrix,

$$[J] = [I - P][I + P]^{-1}[C]. \tag{28}$$

2.3.2. Boundary condition

Generally, the intensity boundary condition is used to calculate the magnitude of the fictitious sources Φ. There are three causes of generated energy flow at the boundary: first, external sources exciting walls; second, energy absorption by the walls; and last, energy exchanges through the boundaries. Therefore, the boundary surfaces can be divided according to the types of boundary condition, which can be expressed as

$$\{q\}_{\Gamma} = \{q\}_{\Gamma_1}^{\text{ext}} + \{q\}_{\Gamma_2}^{\text{abs}} + \{q\}_{\Gamma_3}^{\text{trans}}, \tag{29}$$

where Γ refers to the boundary surfaces composed of external source region Γ_1, absorbent region Γ_2, and coupled boundaries Γ_3; $\{q\}_{\Gamma_1}^{\text{ext}}$ are the external sources; $\{q\}_{\Gamma_2}^{\text{abs}}$ is absorbed energy and $\{q\}_{\Gamma_3}^{\text{trans}}$ is transmitted energy. In the case of the externally excited intensity (i.e. vibrating wall), $\{q\}_{\Gamma_1}^{\text{ext}}$ need to be known before computation, and the power dissipation due to absorption can be calculated as

$$\{q\}_{\Gamma_2}^{\text{abs}} = \frac{c_g}{4}[\alpha]\{e\}_{\Gamma_2}, \tag{30}$$

where α is the absorption coefficient of the boundary surface [24] and c_g indicates group velocity. For coupled domains, the energy exchanges between them can be expressed in a joint matrix using Equation (25), as described previously.

Considering two domains (1 and 2), Equation (8) can be rewritten as

$$\begin{Bmatrix} q_1 \\ q_2 \end{Bmatrix}^{\text{ext}} + \begin{Bmatrix} q_1 \\ q_2 \end{Bmatrix}^{\text{abs}} + \begin{Bmatrix} q_1 \\ q_2 \end{Bmatrix}^{\text{trans}} = \begin{Bmatrix} F_1 & 0 \\ 0 & F_2 \end{Bmatrix} \begin{Bmatrix} \Phi_1 \\ \Phi_2 \end{Bmatrix} + \begin{Bmatrix} F_1^{\text{input}} & 0 \\ 0 & F_2^{\text{input}} \end{Bmatrix} \begin{Bmatrix} \Pi_1 \\ \Pi_2 \end{Bmatrix}, \tag{31}$$

where the left hand side equates to the net energy flow of domains 1 and 2; Φ and Π indicate the magnitude of fictitious sources and acoustic sources, respectively; F and F^{input} are the matrices of the Green's functions for the intensity (Equation 4) between the boundary elements and the fictitious sources, and between the boundary elements and the acoustic sources, respectively; and subscripts 1 and 2 indicate domains 1 and 2, respectively.

In Equation (31), the absorbed energy flow term can be defined as in Equation (32) by using Equation (30), and the transmitted energy flow term can be determined as in Equation (33) by using Equation (27),

$$\begin{aligned} \begin{Bmatrix} q_1 \\ q_2 \end{Bmatrix}^{\text{abs}} &= \frac{c_g}{4} \begin{bmatrix} \alpha_1 & \\ & \alpha_2 \end{bmatrix} \begin{Bmatrix} e_1 \\ e_2 \end{Bmatrix} \\ &= \frac{c_g}{4} \begin{bmatrix} \alpha_1 & \\ & \alpha_2 \end{bmatrix} \begin{bmatrix} G_1 & \\ & G_2 \end{bmatrix} \begin{Bmatrix} \Phi_1 \\ \Phi_2 \end{Bmatrix} \\ &\quad + \frac{c_g}{4} \begin{bmatrix} \alpha_1 & \\ & \alpha_2 \end{bmatrix} \begin{bmatrix} G_1^{\text{input}} & \\ & G_2^{\text{input}} \end{bmatrix} \begin{Bmatrix} \Pi_1 \\ \Pi_2 \end{Bmatrix}, \end{aligned} \tag{32}$$

$$\begin{aligned} \begin{Bmatrix} q_1 \\ q_2 \end{Bmatrix}^{\text{trans}} &= [J] \begin{Bmatrix} e_1 \\ e_2 \end{Bmatrix} \\ &= [J] \begin{bmatrix} G_1 & \\ & G_2 \end{bmatrix} \begin{Bmatrix} \Phi_1 \\ \Phi_2 \end{Bmatrix} \\ &\quad + [J] \begin{bmatrix} G_1^{\text{input}} & \\ & G_2^{\text{input}} \end{bmatrix} \begin{Bmatrix} \Pi_1 \\ \Pi_2 \end{Bmatrix}, \end{aligned} \tag{33}$$

where e_1 and e_2 are the energy densities of the boundary elements; J is the joint matrix which describes the relationship between the energy density and the intensity at the interface; and G and G^{input} are the matrices of the Green's functions for energy density (Equation 3) between the boundary elements and the fictitious sources, and between the boundary elements and the acoustic sources, respectively.

After this, all terms except for the externally excited energy flow component in Equation (31) have Φ vector or Π vector, and so Equation (31) can be written in a simpler form as

$$A \begin{Bmatrix} \Phi_1 \\ \Phi_2 \end{Bmatrix} = - \begin{Bmatrix} q_1 \\ q_2 \end{Bmatrix}^{\text{ext}} - B \begin{Bmatrix} \Pi_1 \\ \Pi_2 \end{Bmatrix}, \tag{34}$$

where A and B are given in the two equations

$$\begin{aligned} A &= \frac{c_g}{4} \begin{bmatrix} \alpha_1 & \\ & \alpha_2 \end{bmatrix} \begin{bmatrix} G_1 & \\ & G_2 \end{bmatrix} \\ &\quad + [J] \begin{bmatrix} G_1 & \\ & G_2 \end{bmatrix} - \begin{bmatrix} F_1 & \\ & F_2 \end{bmatrix}, \end{aligned} \tag{35}$$

$$\begin{aligned} B &= \frac{c_g}{4} \begin{bmatrix} \alpha_1 & \\ & \alpha_2 \end{bmatrix} \begin{bmatrix} G_1^{\text{input}} & \\ & G_2^{\text{input}} \end{bmatrix} \\ &\quad + [J] \begin{bmatrix} G_1^{\text{input}} & \\ & G_2^{\text{input}} \end{bmatrix} - \begin{bmatrix} F_1^{\text{input}} & \\ & F_2^{\text{input}} \end{bmatrix}. \end{aligned} \tag{36}$$

The magnitude of the fictitious sources Φ on the boundaries can be computed by multiplying Equation (34) by the inverse of A, then the energy density of any receiving points can be simply calculated by Equation (7). Using the above procedure, the number of domains is not restricted, thus many domains can be calculated simultaneously by considering the coupling effect.

3. Results and Discussion

3.1. The small reverberation chamber

A coupled small reverberation chamber with a common partition of 1.2 m^2 was used to determine the sound reduc-

Document downloaded by @DAEL, 2026-11-06 14:24:34 - personal use only

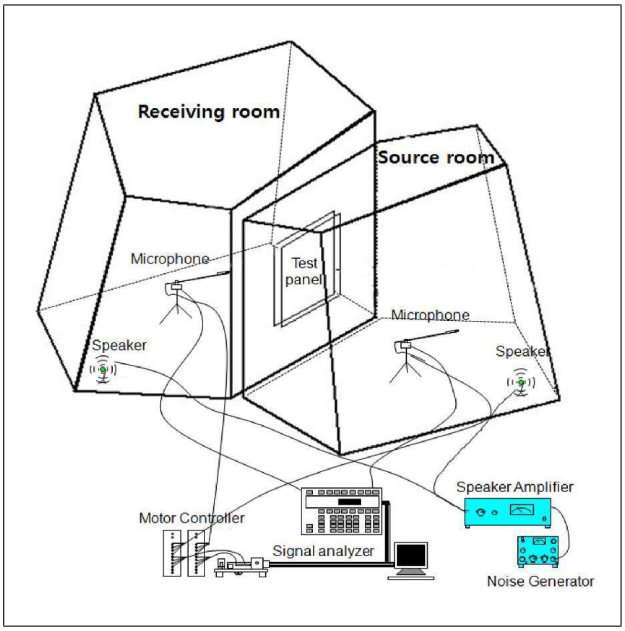


Figure 2. An experimental set-up for the measurement of sound reduction index by using coupled small reverberation chamber (Volume of receiving room: 3.252 m^3, Area of test panel: 1.2 m^2).

tion index (SRI) of a partition (the setup was as in Figure 2). A rotating microphone in each room measured the sound pressure level at six points according to the rotating angle step of 60°.

A 0.6 mm steel plate was used as a test panel and the boundary element model for the simulation was prepared as in Figure 3. To obtain the power transmission coefficient, the official (certified) test results of the SRI for 0.6 mm steel plates was used, and the equation of the relationship between the SRI and the power transmission coefficient is [25]

$$\mathrm{TL} = -10\log_{10}(\tau). \tag{37}$$

The averaged absorption coefficients were calculated through the reverberation time T_{60} of the receiving rooms; they were very small and so a reliable frequency range needed to be considered before the test results were recorded.

The noise response in a room is divided into two regions according to the frequency. The Schroeder frequency defined in Equation (38) is sometimes helpful although it is quite restrictive [26, 27],

$$f_c = 2000\sqrt{T_{60}/V}. \tag{38}$$

Below the Schroeder frequency, the modal density is insufficient and the room noise field is decided by normal modes, thus energy-based methods are inadequate for those frequencies. On the other hand, at frequencies above the Schroeder frequency, the noise field becomes uniform by overlapping many normal modes, and so statistics/energy based methods are applicable to these frequencies.

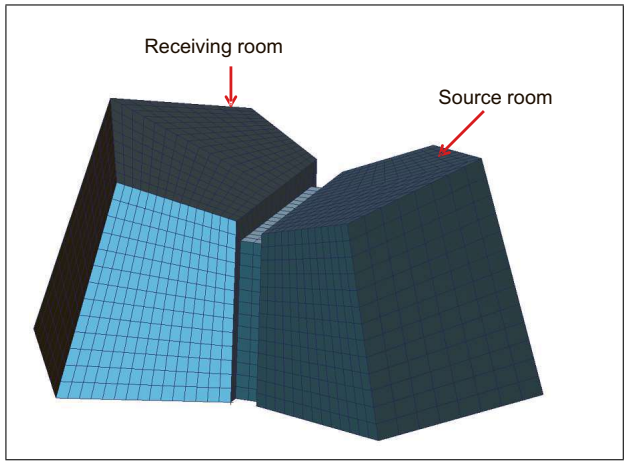


Figure 3. Boundary element model of coupled small reverberation chamber (The number of element: 3616).

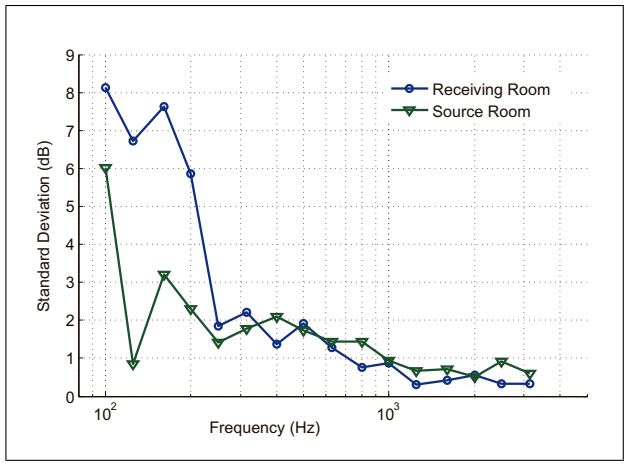


Figure 4. (Colour online) Standard deviation for the spatial distribution of sound pressure (blue solid line: receiving room, green solid line: source room).

In this study, the Schroeder frequency of the receiving room is about 800 Hz, which means that the sound field below 800 Hz may not be uniform. The standard deviations for the spatial distribution of sound pressure levels (six points) are shown in Figure 4 and Table I, and as can be seen in the figure, it decreases rapidly as the frequency increases.

Error calculations between the analysis and measurements in the receiving room are shown in Table II, and it is acceptable to conclude that simulation results are reliable above 500 Hz. As mentioned previously, the test room is too small to apply the energy-based method to estimate the sound pressure field at frequencies below 500 Hz (sometimes the Schroeder frequency formula gives a higher value than the actual frequency limit [27]).

The SRI curve for the test panel is shown in Figure 5, where SRI is defined as

$$\mathrm{SRI\ [dB]} = L_1 - L_2 + 10\log_{10}(S/A), \tag{39}$$

where L_1 and L_2 are the space-averaged sound pressure levels in the source and receiving rooms, respectively; S

Document downloaded by @DAEL, 2026-11-06 14:24:34 - personal use only

Table I. Measured sound pressure levels in the small reverberation rooms (Spatial average, 6 points). All values in dB, Frequencies in Hz.

	Receiving room			Source room		
Freq	Aver	Range	Dev	Aver	Range	Dev
100	69.49	18.06	8.12	87.26	15.07	6.02
125	79.86	17.71	6.72	91.78	2.67	0.86
160	72.69	19.03	7.62	89.80	9.64	3.21
200	77.19	14.90	5.85	90.88	5.80	2.30
250	78.03	5.78	1.85	97.11	3.66	1.42
315	77.01	6.84	2.20	96.48	4.97	1.78
400	77.84	3.90	1.38	94.82	6.44	2.10
500	70.90	5.55	1.91	93.38	5.21	1.74
630	70.35	3.35	1.27	90.80	4.35	1.45
800	66.10	2.35	0.77	87.18	4.70	1.45
1000	66.75	2.67	0.87	89.84	2.59	0.94
1250	71.87	0.99	0.31	95.29	1.89	0.66
1600	69.71	1.12	0.43	95.68	2.23	0.71
2000	67.28	1.73	0.55	95.13	1.42	0.52
2500	64.97	0.98	0.33	95.23	2.80	0.92
3150	59.20	1.04	0.33	92.00	1.87	0.60

Table II. Error between simulated and measured sound pressure level in receiving room (Error(%) $= |A - B|/B \cdot 100$, A: simulation, B: measurement).

	Rotating Angle (degree)					
Freq	0	60	120	180	240	300
100	31.47	0.45	0.97	18.44	1.08	1.11
125	1.62	14.06	6.47	9.53	3.95	12.15
160	0.96	27.63	0.90	3.39	3.20	23.24
200	5.66	11.50	1.41	3.93	5.71	13.74
250	6.74	5.83	8.35	7.54	0.61	5.72
315	5.52	2.59	10.17	2.45	0.59	2.92
400	1.38	2.57	1.92	0.68	1.01	1.54
500	2.47	7.76	3.14	5.17	9.17	8.34
630	0.70	0.02	0.00	4.17	2.78	0.47
800	2.43	2.44	1.22	2.31	0.59	0.71
1000	3.32	1.32	0.69	3.41	0.70	3.00
1250	0.21	0.90	0.83	1.94	1.32	0.11
1600	0.22	0.99	0.14	1.30	0.35	0.27
2000	1.34	1.11	0.09	1.14	2.06	0.14
2500	1.60	0.56	0.34	0.57	0.62	2.03
3150	1.44	1.88	0.53	0.32	0.24	0.85

is the area of common partition, and A is the absorption area of the receiving room obtained by the product of the absorption coefficient and the surface area of the room [25]. Moreover, the comparison between the analysis and measurements shows good agreement, especially above 500 Hz.

3.2. Cabin unit mock-up

For a second validation example, the cabin unit mock-up was used to validate the proposed method. Generally, a mock-up system is built to confirm that the SRI value between two spaces (such as cabin-to-cabin and cabin-to-corridor) is acceptable before the construction of a ship

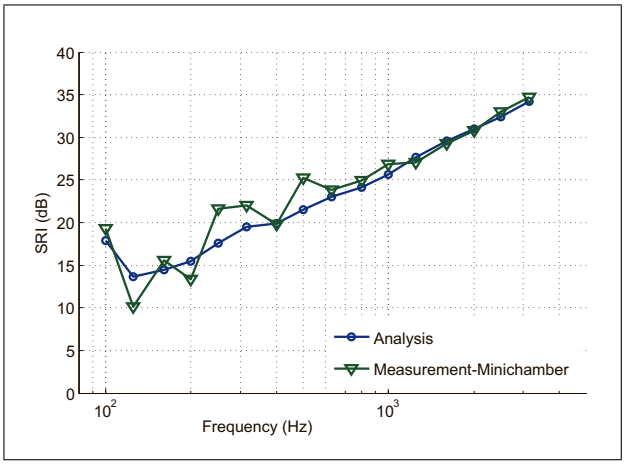


Figure 5. (Colour online) Comparison of SRI between analysis and measurement (blue solid line: analysis, green solid line: measurement).

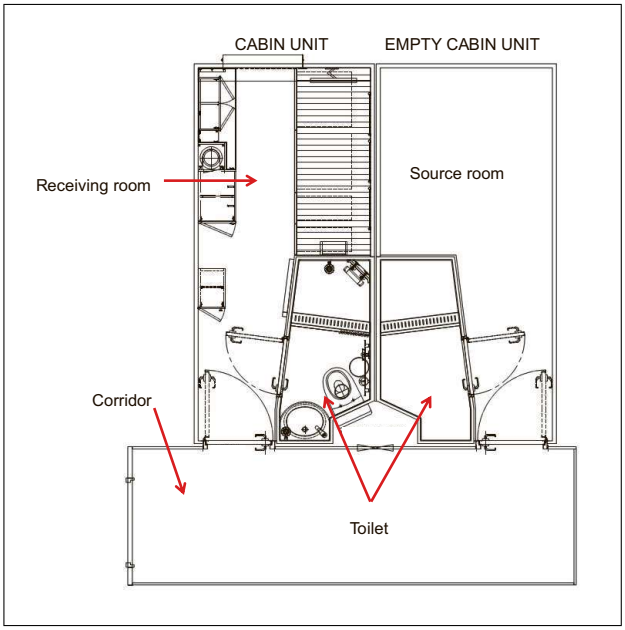


Figure 6. Unit cabin mock-up system.

or offshore structure because there are some rules limiting the SRI level for quiet cabins. Compared with previous experimental systems, the mock-up system consisted of five domains, as shown in Figure 6, and the 3D BEM models were prepared as depicted in Figure 7 (the dimensions of the cabin were calculated as $L \times B \times H = 4.185\,\text{m} \times 1.93\,\text{m} \times 2.3\,\text{m}$). All of the possible energy transmission paths such as door, wall, and ceiling were considered by modeling their power transmission and reflection coefficients obtained through certified laboratory test results of TL (Transmission Loss) (shown in Figure 8 for each building component); the double panels were for the common wall between the rooms and the single panels were for the othe r walls. The averaged absorption coefficients for the receiving room were computed using the measured reverberation time.

Figure 9 shows the spatial distribution of the energy density at 3.15 kHz. As can be seen in the figure, the sound

Document downloaded by @DAEL, 2026-11-06 14:24:34 - personal use only

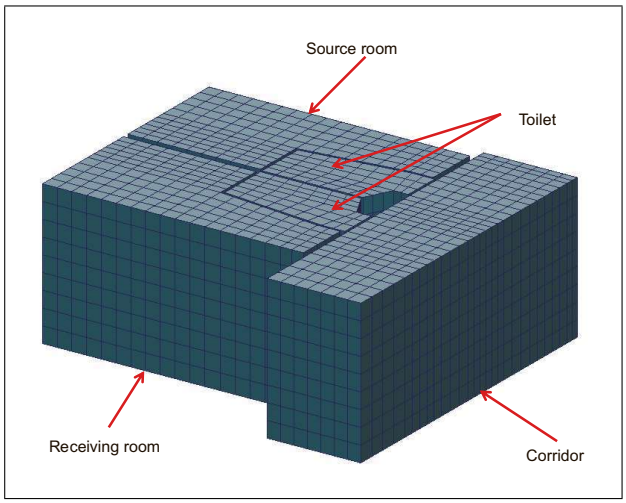


Figure 7. 3D BE models.

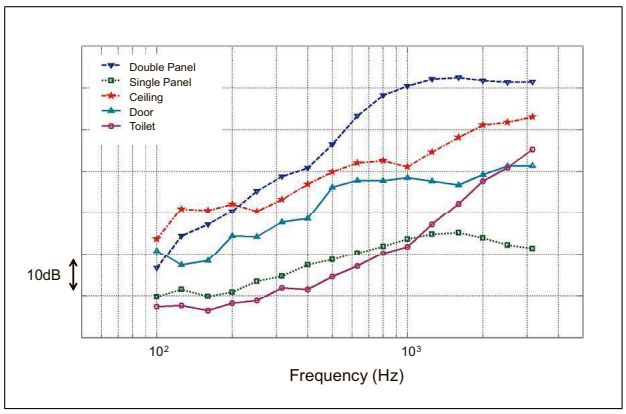


Figure 8. Sound reduction index (Laboratory test).

Table III. The maximum and the minimum values of each space (3.15 kHz).

Space	Max. (dB)	Min. (dB)
Source room	110.13	101.46
Receiving room	40.38	37.46
Toilet (source room side)	56.89	53.77
Toilet (receiving room side)	36.03	31.07
Corridor	69.48	61.66

energy was generated in the source room and propagated to the corridor, the next room, and the toilet. After this, the sound energy of each domain affected each other until they reached a steady state. The maximum and minimum values in each domain are reported in Table III.

The cabin unit mock-up was built and fully outfitted. The sound pressure levels were measured at 10 points in each room and space-averaged values were used to calculate the SRI values according to ISO 717-1(1996) guidelines [28]. Finally the SRI values for all frequencies (1/3-octave band center frequencies from 100 Hz to 3.15 kHz) were obtained. As seen in the Figure 10, there is good agreement but with some errors because the mock-up facility is not like the reverberation chamber; it has additional equipment such as ventilation ducts, electrical systems (the same as in the real ships) that can affect the SRI values. Nevertheless, the method gave fairy good results.

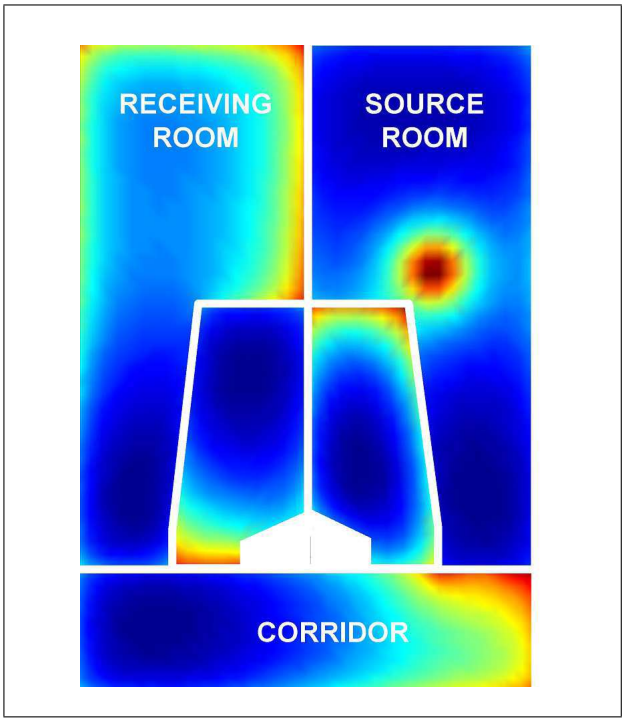


Figure 9. Energy density distribution of cabin unit mock-up system (height = 1.5 m).

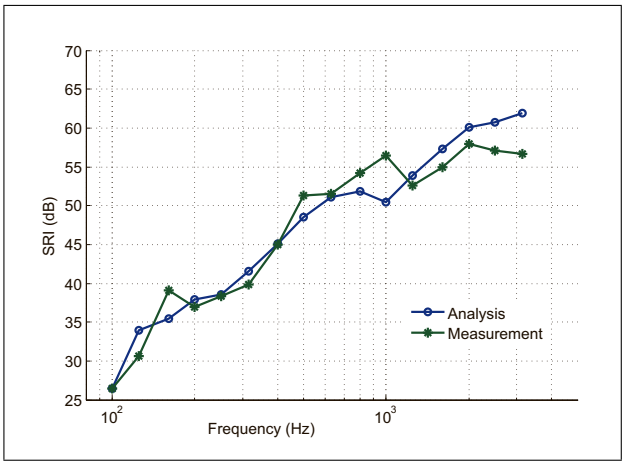


Figure 10. (Colour online) Comparison of sound reduction index (Rw) of adjoining cabins (blue solid line: analysis, red solid line: measurement).

It is difficult to estimate the SRI of the cabin units because the sound energy transmits through multiple paths. Therefore, this multi-domain method could be a reliable solution.

4. Conclusion

In this paper, an indirect EFBEM approach to solve three-dimensional multi-domain problems considering energy exchanges among a number of adjoining domains was developed. This research deals with a newly developed

Document downloaded by @DAEL, 2026-11-06 14:24:34 - personal use only

procedure incorporating the derivation of a boundary element matrix equation with a joint matrix and three different types of boundary conditions, i.e. vibrating walls, energy absorbing walls, and energy transmitting walls. Compared with the direct method, which is derived with a plane wave assumption and the divergence theorem, the indirect method is useful for almost all acoustic situations, including sound radiation, and for all types of domain because the Green's function for spherical waves can be applied. To validate the method, a comparison between the numerical analysis and experimental results for a small reverberation chamber and a unit cabin mock-up system was carried out. The SRI results of which showed good agreement.

In conclusion, the method is a reliable way to solve large and complex acoustic models which have many coupled domains.

Acknowledgement

This study was partially supported by the program for Leading Industry Development for Economic Region funded by the Ministry of Knowledge Economy (A002200322). The authors would like to thanks BIP Industry Co., Ltd. for production of the cabin unit mock-up facility.

References

[1] R. H. Lyon: Statistical Energy Analysis of Dynamical Systems. MIT Press, Cambridge, 1975.

[2] V. D. Belov, S. A. Rybak, B. D. Tartakovskii: Propagation of vibrational energy in absorbing structures. Journal of Soviet Physics Acoustics **23**(2) (1977) 115–119.

[3] D. J. Nefske, S. H. Sung: Power flow finite element analysis of dynamic systems: basic theory and application to beams. Journal of Vibration, Acoustics, Stress and Reliability in Design **111** (1989) 94–100.

[4] J. C. Wohlever, R. J. Bernhard: Mechanical energy flow models of rods and beams. Journal of Sound and Vibration **153** (1973) 1–19.

[5] O. M. Bouthier, R. J. Bernhard: Simple models of the energetics of transversely vibrating plates. Journal of Sound and Vibration **182** (1995) 149–164.

[6] O. M. Bouthier, R. J. Bernhard: Simple models of energy flow in vibrating membranes. Journal of Sound and Vibration **182** (1995) 129–147.

[7] M. J. Smith: A hybrid energy method for predicting high frequency vibrational. Journal of Sound and Vibration **202**(3) (1997) 375–394.

[8] A. Le Bot: A vibroacoustic model for high frequency analysis. Journal of Sound and Vibration **211** (1998) 537–554.

[9] D. H. Park, S. Y. Hong, H. G. Kil, J. J. Jeon: Power flow model and analysis of in-plane waves in finite coupled thin plates. Journal of Sound and Vibration **244** (2001) 651–668.

[10] S. H. Seo, S. Y. Hong, H. G. Kil: Power flow analysis of reinforced beam-plate coupled structures. Journal of Sound and Vibration **259** (2003) 1109–1129.

[11] Ho-Won Lee, Suk-Yoon Hong, Do-Hyun Park, Hyun-Wung Kwon: Energy flow boundary element method for vibration analysis of one and two dimension structures. Shock and Vibration **15** (2008) 33–50.

[12] Hyun-Wung Kwon: Development of PFBEM Indirect Method for the Analysis of Radiating Noise Problems. Ph.D. Dissertation, Seoul Nat'l University. 2004.

[13] Hyun-Wung Kwon, Suk-Yoon Hong, Jee-Hun Song: Development of indirect EFBEM for radiating noise analysis including underwater problems. International Journal of Naval Architecture and Ocean Engineering **5**(3) (2013) 392–403.

[14] A. Wang, N. Vlahopoulos, K. Wu: Development of an energy boundary element formulation for computing high-frequency sound radiation from incoherent intensity boundary conditions. Journal of Sound and Vibration **278** (2004) 413–436.

[15] Jerry Rouse, Linda Franzoni: Improvement of a high–frequency broadband energy-intensity boundary element method to include high resolution specular reflection. Journal of Computational Acoustics **13**(1) (2005) 99–125

[16] Sebastien Besset, Mohamed Ichchou, Louis Jezequel: A coupled BEM and energy flow method for mid–high frequency internal acoustic. Journal of Computational Acoustics **18** (1) (2010) 69–85.

[17] D. J. Chappell, S. Giani, G. Tanner: Dynamical energy analysis for built-up acoustic systems at high frequencies. The Journal of the Acoustical Society of America **130** (3) (2011) 1420–1429

[18] Suk-Yoon Hong, Hyun-Wung Kwon, Jong-Do Kim: Car Interior and Exterior Multi-domain Noise Analysis using Energy Flow Analysis (EFA) Software, NASEFAC++. Proceedings of SAE international, 2007-01-2174.

[19] Jong-Do Kim, Suk-Yoon Hong, Ho-Won Lee: Hyun-Wung Kwon: Car Interior and Exterior Multi-domain Noise Analysis using Power Flow Boundary Element Method. Proceedings of the KSNVE Annual Spring Conference, 2007, 489–493.

[20] Jong-Do Kim, Suk-Yoon Hong, Hyun-Wung Kwon: Interior and exterior multi-domain noise analysis using EFBEM. Proceedings of TEAM, 2007, 85–92.

[21] Jong-Do Kim, Suk-Yoon Hong, Jee-Hun Song: Development of Power Flow Boundary Element Method for 3-Dimensional Multi-domain Noise Analysis. Transactions of the Korean Society for Noise and Vibration Engineering **21**(10) (2011) 967–974.

[22] Hyun-Wung Kwon, Suk-Yoon Hong, Ho-Won Lee, Jee-Hun Song: Power flow boundary element analysis for multi-domain problems in vibrational built-up structures. Journal of Sound and Vibration **330** (2011) 6482–6494.

[23] Jong-Do Kim, Suk-Yoon Hong, Hyun-Wung Kwon, Jee-Hun Song: Energy flow model considering near field energy for predictions of acoustic energy in low damping medium. Journal of Sound and Vibration **330** (2011) 271–286.

[24] Tor Erik Vigran: Building acoustics, Taylor & Francis, New York, 2008.

[25] J. D. Irwin, E. R. Graf: Industrial noise and vibration control. Prentice Hall, New Jersey, 1979.

[26] Seyed Mostafa Khezri, Pedram Jafari Halkouhi: The Schroeder frequency of furnished and unfurnished space. Romanian Journal of Acoustics and Vibration **9**(2) (2012) 113–116.

[27] Ramani Ramakrishnan, Anant Grewal: Reverberation rooms and spatial uniformity. Canadian Acoustics **36**(3) (2008) 28–29.

[28] ISO 717–1: Acoustics – Rating of sound insulation in buildings and of buildings elements. Part 1: Airborne sound insulation. International Organization for Standardization, Genève, 1996.

Document downloaded by @DAEL, 2026-11-06 14:24:34 - personal use only